

High resolution retinal imaging with a compact adaptive optics spectral domain optical coherence tomography system

Daniel X. Hammer*^a, Nicusor V. Iftimia^a, Chad E. Bigelow^a, Teoman E. Ustun^a, Benjamin Bloom^a, R. Daniel Ferguson^a, and Stephen A. Burns^b

^aPhysical Sciences Inc., 20 New England Business Center, Andover MA 01810

^bDepartment of Optometry, Indiana University, Bloomington IN 47405

ABSTRACT

Adaptive optics (AO) is used to correct ocular aberrations primarily in the cornea, lens, and tear film of every eye. Among other applications, AO allows high lateral resolution images to be acquired with scanning laser ophthalmoscopy (SLO) and optical coherence tomography (OCT). Spectral domain optical coherence tomography (SDOCT) is a high-speed imaging technique that can acquire cross-sectional scans with micron-scale axial resolution at tens to hundreds of kHz line rates. We present a compact clinical AO-SDOCT system that achieves micron-scale axial and lateral resolution of retinal structures. The system includes a line scanning laser ophthalmoscope (LSLO) for simultaneous wide-field retinal viewing and selection of regions-of-interest. OCT and LSLO imaging and AO correction performance are characterized. We present a case study of a single subject with hyper-reflective lesions associated with stable, resolved central serous retinopathy to compare and contrast AO as applied to scanning laser ophthalmoscopy and optical coherence tomography. The two imaging modes are found to be complementary in terms of information on structure morphology. Both provide additional information lacking in the other. This preliminary finding points to the power of combining SLO and SDOCT in a single research instrument for exploration of disease mechanisms, retinal cellular architecture, and visual psychophysics.

Keywords: Adaptive optics, spectral domain optical coherence tomography, scanning laser ophthalmoscopy, retinal imaging, ophthalmology, ocular aberrations, wavefront sensor, deformable mirror

1. INTRODUCTION

Adaptive optics (AO) has recently been applied to ophthalmic imaging systems to correct ocular aberrations and to provide a higher transverse resolution than can be achieved absent adjustment for aberrations [1-2]. AO systems use a wavefront sensor (WS) to detect and measure ocular aberrations and a deformable mirror (DM) to manipulate the wavefront to achieve near-diffraction-limited focusing in the eye. The WS and DM are usually elements in a feedback control loop for dynamic correction of optical distortions arising from tear film. For scanning laser ophthalmoscopy, AO enables *in-vivo* resolution of the photoreceptor cone mosaic [3], leukocytes [4], the foveal avascular zone [5], and retinal pigment epithelial (RPE) mosaic [6], among other retinal structures and cells. However, even with diffraction-limited focus, the eye's numerical aperture limits depth sectioning to a depth-of-field of 75-100 μm at best [7].

Optical coherence tomography (OCT) uses low coherence interferometry techniques to achieve superb depth sectioning to several microns axial resolution. This type of instrument has allowed routine examination and collection of high-resolution cross-sectional scans of retinal layers. AO has recently been applied to time-domain and high-speed spectral domain OCT systems to increase signal and resolution in various retinal layers [8-10]. However, by its nature, spectral domain OCT collects information more slowly in the *en-face* plane, and thus presents a challenge for imaging structures such as the cone mosaic [10]. Moreover, SDOCT is not suited for some advanced imaging techniques, for example to collect autofluorescence signals from lipofuscin. Thus, we view adaptive optics scanning laser ophthalmoscopy (AOSLO) and adaptive optics spectral domain optical coherence tomography (AO-SDOCT) as complementary. Both have achieved impressive results for diagnosis of retinal disease, for exploring and understanding the complete cellular architecture of vision and its development, and for assisting in the development of novel drug and gene-based treatment methods. However, both have inherent deficiencies that may restrict their capabilities. The full picture for clinical or research applications may only come by combination of SLO and OCT techniques.

In this paper, we present the development of a compact AO-SDOCT instrument suitable for clinical use. We also discuss the combined application of AO-SDOCT and AOSLO for retinal disease diagnosis and examination. This is done via case study, where a subject with stable lesions that developed during central serous retinopathy, was imaged both with AO-SDOCT and with AOSLO. This case study highlights the advantages and disadvantages of both techniques and points toward further engineering and development that may yield a more ideal imaging instrument.

2. METHODS

2.1 Optical Setup

The AO-SDOCT optical setup is shown in Fig. 1. The system has been described in detail elsewhere [11] and is covered here only briefly. The major components are the line scanning laser ophthalmoscope (LSLO), spectral domain optical coherence tomography (SDOCT) interferometer and spectrometer, Hartmann-Shack wavefront sensor (WS) and deformable mirror (DM). The fixation target is an 8×8 LED that communicates to the computer via serial line.

The LSLO provides wide-field (~20-deg) retinal images [12] for selection of targets or regions for further examination with the high-resolution SDOCT component. The LSLO beam uses a 735-nm laser diode and delivers less than 500- μ W of power to the retina in a focused line. A linear array detector (Dalsa Inc.) collects the back-scattered LSLO light. The LSLO uses custom scan and detector objectives (O1 and O2) to correct chromatic aberration and achieve good field flatness.

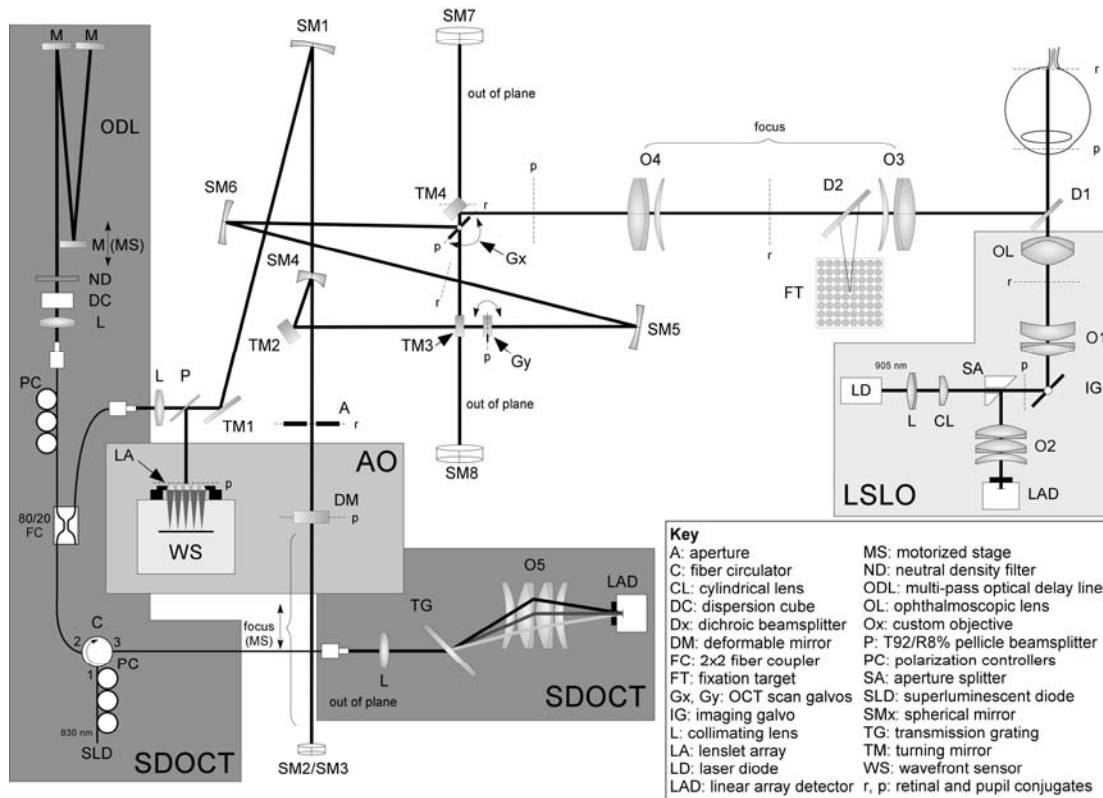


Fig. 1. Optical setup of the compact AO-SDOCT system. Main components include line scanning laser ophthalmoscope (LSLO), SDOCT interferometer and spectrometer, Hartmann-Shack wavefront sensor and deformable mirror.

The SDOCT setup is configured in a typical arrangement with matched sample and reference paths and spectrometer in the detection path. The optical delay line compactly folds the 2.55-m SDOCT optical path. The scan optics primarily use spherical mirrors to relay the pupil to five conjugates for the x - y scan galvanometers, DM, and WS. The first pupil conjugate can be used for trial lenses for subjects that require large spherical correction. Custom objectives are used in the first lens relay (O3 and O4) and the SDOCT spectrometer (O5). A 1200 lp/mm transmission grating and 2048-pixel

linear array detector (Atmel Inc.) are used in the spectrometer. An 80/20 fiber coupler is used in the interferometer. Polarization controllers and a circulator are used to maximize throughput. A cube is used in the reference path to compensate dispersion in the sample path optics and eye. A Broadlighter superluminescent diode (Superlum Inc.) at 830 ± 30 nm achieves ~ 4 μ m axial resolution in the eye. The OCT beam delivers less than 400- μ W of power to the retina.

The WS uses a 65×65 lenslet array and 1024×1024 pixel, 12-mm CCD camera (Dalsa Inc.). A MEMS-based DM (Boston Micromachines Inc.) with 141 actuators and a ~ 4 μ m stroke is used for wavefront correction. A pellicle beamsplitter directs a portion of the OCT return beam to the wavefront sensor.

2.2 Instrumentation

A block diagram of the system instrumentation is shown in Fig. 2. The deformable mirror (DM) uses high-voltage drive electronics and a single PCI digital card to drive all actuators. Two CameraLink framegrabbers (National Instruments Inc.) are used to acquire images from the WS, LSLO, and SDOCT cameras (the PCI-1430 is capable of acquiring images from two cameras). Two computer-controlled stages (Velmex Inc.) are used to position the optical delay line mirror (for coherence range) and the DM mirror stage (for focus). Software drivers allow these stages to operate either independently or locked together so that the coherence range can remain fixed while focus is adjusted.

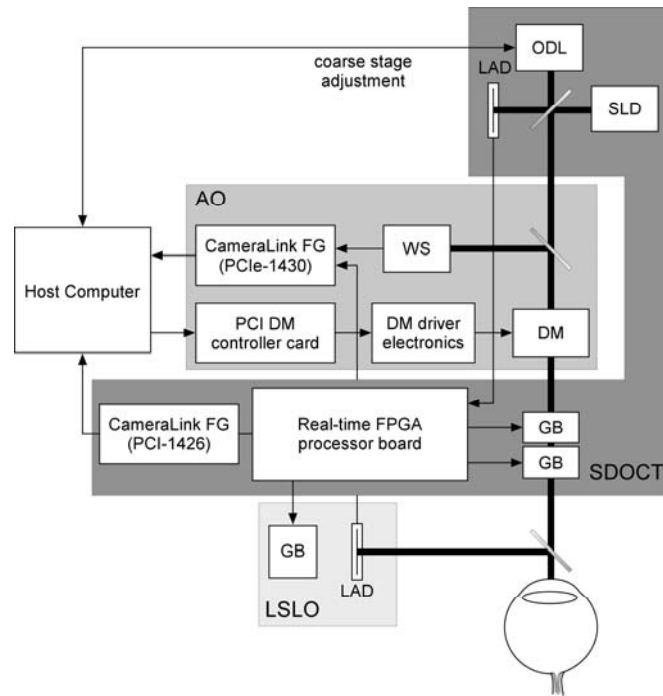


Fig. 2. Instrumentation setup for the compact AO-SDOCT system. Acronyms are as in Fig. 1 with GB: galvanometer board and FG: framegrabber.

A slightly modified version of this layout is currently used pending final completion of the development of a custom real-time SDOCT image processing board. Further details on the design and implementation of the real-time SDOCT image processing board can be found in these proceedings [13]. In lieu of this custom board, a USB data acquisition controller is used to drive the galvanometers.

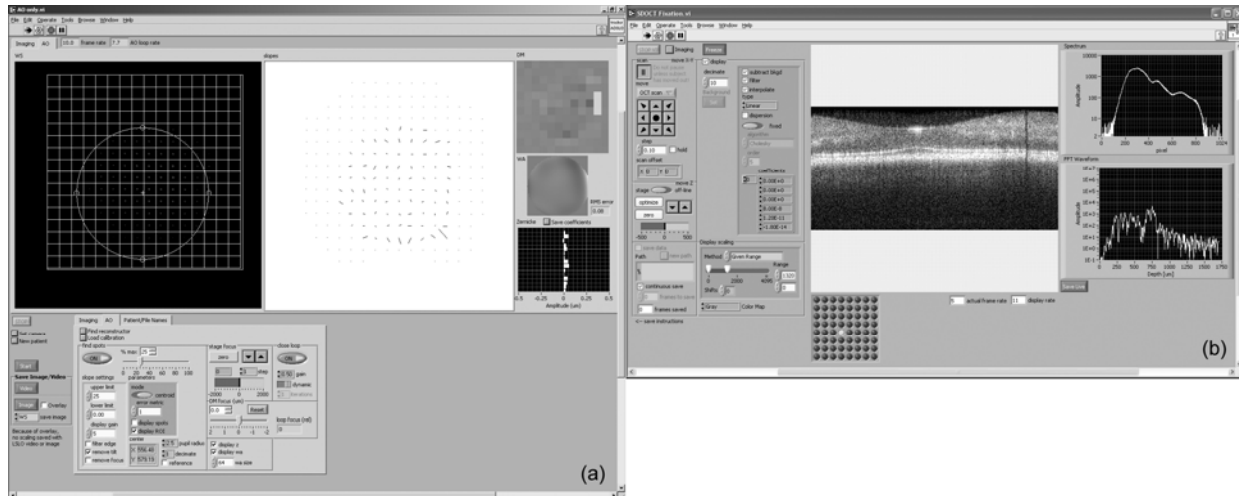


Fig. 3. Acquisition user interface for AO/LSLO computer (a) and SDOCT computer (b).

Both controller computers operate custom acquisition and analysis software written in LabVIEW (National Instruments Inc.), Matlab (Mathworks Inc.), and C/C++. The primary computer controls acquisition and processing of WS and LSLO images, control of the DM, and other AO processing and display (e.g., calculation of wavefront error map, RMS wavefront error, Strehl ratio, and Zernike coefficients). The second computer performs all SDOCT image acquisition and processing. Completion of the custom real-time processing board development in early-spring 2007 will obviate the need for the second computer. The user interfaces for the current software are shown in Fig. 3.

2.3 Subjects

Seven volunteers (4 men, 3 women) have been tested to date. In this paper, we present images and results from 3 subjects. One subject had a resolved (i.e., stable) case of central serous retinopathy. All other subjects had normal eyes without disease. Informed consent was obtained prior to image acquisition according to our Institutional Review Board (IRB)-approved protocol. Subjects were typically imaged for about one hour to collect a variety of line and raster scans. The subjects were dilated with a mydriatic agent (0.8% tropicamide/5% phenylephrine) to accept the full diameter of the OCT beam and to maximize the effects of AO on the corrected performance in the eye. The subjects were positioned with a 3-axis stage equipped with a bite bar and head-rest.

3. RESULTS

The system performance was characterized in terms of qualitative LSLO and SDOCT imaging performance and AO correction. We have previously shown an improvement of 3-10 dB in signal-to-noise ratio with AO correction for all subjects [11]. Figure 4 shows LSLO and OCT images from 3 subjects. The SDOCT cross-sectional scans are centered on the fovea. For subjects 1 and 2 the line extends 6.5 deg and for subject 3 it extends 5.2 deg. The LSLO raster scans extend ~19 deg. across the retina. This field of view is enough to image the entire macula or include the fovea and most of the optic disc.

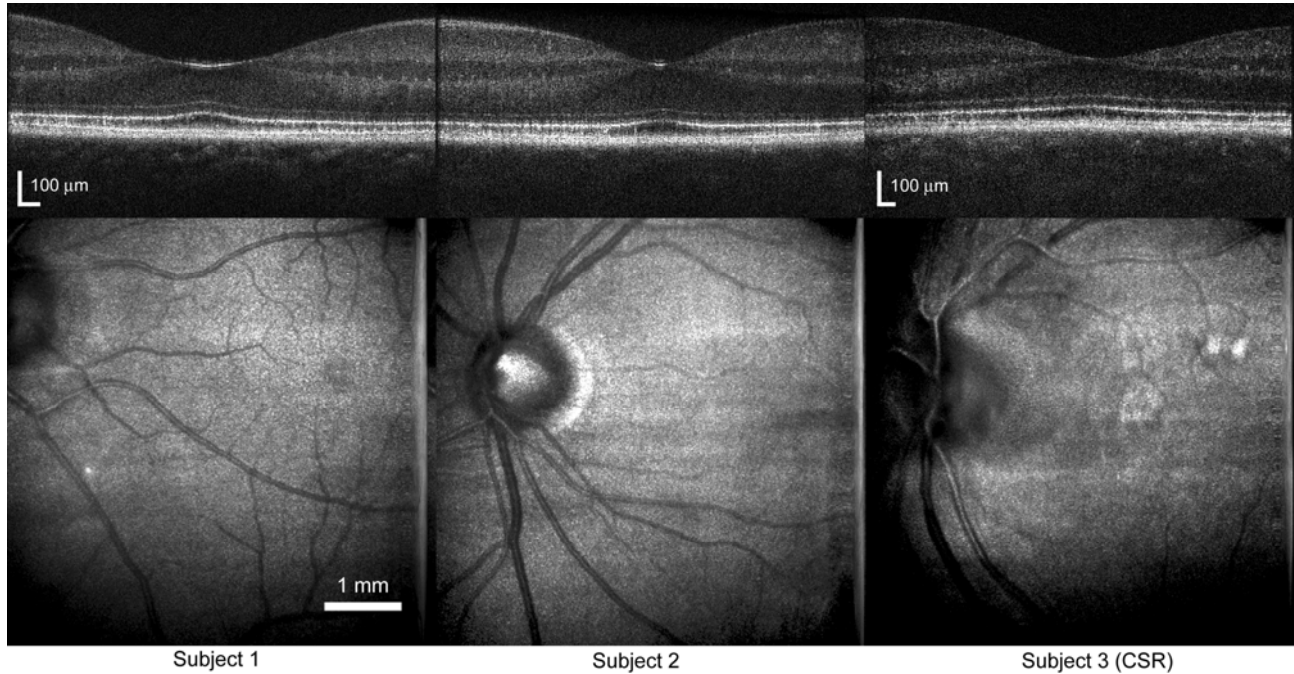


Fig. 4. Single AO-SDOCT (upper row) and LSLO (lower row) images acquired from three subjects.

The SDOCT foveal scans show good resolution of all retinal layers and penetration into the choroid. The single frames show a continuous external limiting membrane across the entire image. Resolution of structures in the photoreceptor layer and vessels and capillaries in the ganglion cell and inner nuclear layers are also apparent. The LSLO images also show high contrast resolution of retinal features commensurate with the field of view. The foveal reflex is visible in subject 1. The bright lamina cribrosa layer in the optic disc is visible in subject 2. Signals from within the lumen of the large vessels are visible in all three subjects.

The adaptive optics performance is summarized in Fig. 5, showing OCT scans, wavefront error maps, and point spread functions with (left column) and without (right column) AO correction. With AO, the RMS wavefront error typically decreased to ~ 0.1 for most subjects. The temporal profile of the RMS wavefront error is shown in Fig. 5g. The closed loop bandwidth, determined from the 10-90% risetime of the curve in Fig. 5g, is 4 Hz. Fig. 5h shows the correction as a function of Zernike order. RMS error decreased for all orders up to 7.

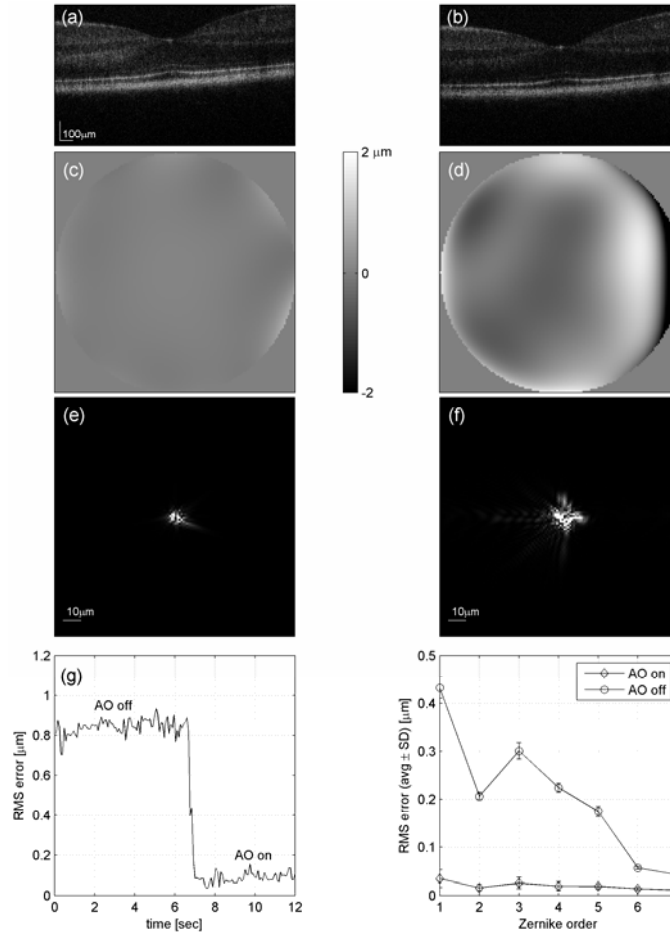


Fig. 5. Adaptive optics performance and its effect on wavefront aberrations. The left column contains data with AO correction (a, c, e) while the right column illustrates system performance without AO (b, d, f). (a) and (b) are representative SDOCT images acquired with AO on and off, respectively. The corresponding wavefront error maps are shown ((c) and (d)) as are the calculated point spread functions ((e) and (f)). The temporal profile of the RMS error is shown in (g) and the average RMS error (for all frames with AO on and off) as a function of Zernike coefficient order is displayed in (h).

4. CASE STUDY: CENTRAL SEROUS RETINOPATHY

To illustrate the complementary nature of AOSLO and AO-SDOCT, we imaged the lesions of the subject with stable CSR with both modes. The AOSLO images were acquired from the system at Indiana University, which is equipped with a retinal tracker (tAOSLO) [14]. The wide field LSLO image of the lesions is shown in Fig. 6, which also shows the approximate location of the scans in Figs. 7-9. In the wide-field LSLO image, these lesions are hyper-reflective, but no information about the source of hypopigmentation or integrity of individual layers can be gleaned from the low resolution image.

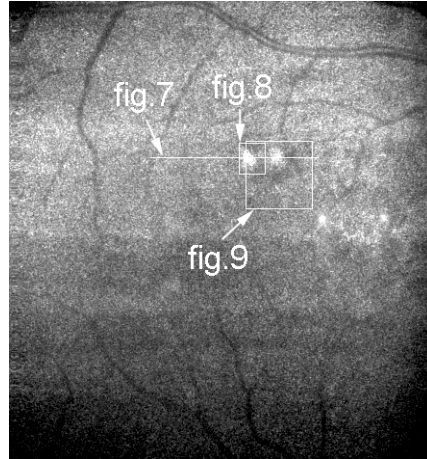


Fig. 6. LSLO image of lesions showing approximate location of scans for Figs. 7-9.

Cross-sectional SDOCT scans (6.5 deg.) through the lesions are displayed in Fig. 7. Shown are a single image and a composite image generated from 11 co-aligned frames. The composite image shows a reduction in speckle. From the depth-resolved OCT scan, we can begin to gather information about the lesions. First, it is apparent that they are not drusen as there is no elevation of the RPE layer. The lesion thickness encompasses the entire thickness of the photoreceptor, RPE, and choriocapillaris layers. The external limiting membrane is elevated, but the anterior plexiform, nuclear, ganglion, and nerve fiber layers appear to be unaffected. The integrity of the photoreceptor layer cannot be determined from the cross-sectional OCT images.

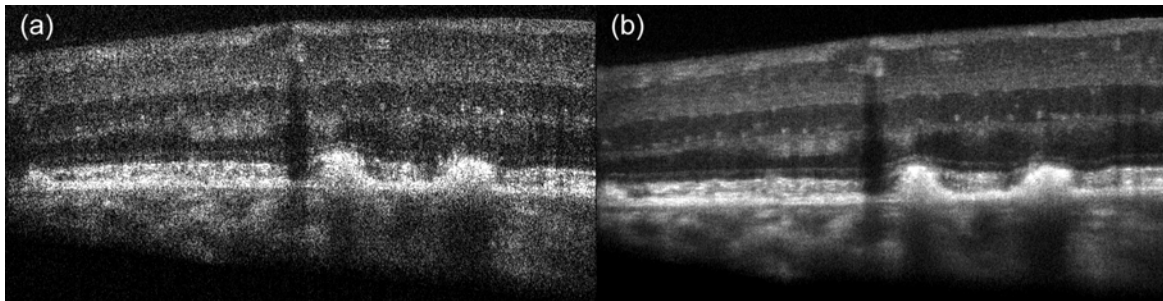


Fig. 7. 6.5-deg. cross-sectional AO-SDOCT scan through lesions: (a) single frame, (b) composite image of 11 aligned and co-added frames.

A montage of *en-face* AOSLO raster scans ($\sim 0.8 \times 1$ deg.) at various retinal depths through the left lesion is shown in Fig. 8. From Fig. 8a, it is clear that there are still large patches of photoreceptors within the lesions. Although microperimetry is necessary to determine the viability of these cones, there doesn't appear to be any diminution of their wave-guiding properties. There are several patches without cones, but these are dark and not the source of the hypopigmentation seen in the wide-field LSLO images. Multiple-scattered light, which is probably the predominate source of the LSLO hyper-reflectance, appears to arise from layers above the photoreceptors. This conclusion is not inconsistent with the conclusions drawn from Fig. 7, because OCT primarily detects single-scattered light.

A montage created from an AO-SDOCT raster scan at various retinal depths through the lesions and surrounding tissue is shown in Fig. 9. During the acquisition of this raster, the AO focus was set to the photoreceptor layer. The analysis software was configured to orient the sliced plane at any angle with respect to the cross-sectional raster scans. This allowed resolution of complete layers that were at acute angles with respect to the fly-through plane. For example, in Fig. 9d, to visualize capillaries across the entire *en-face* image, the fly-through plane is tilted with respect to normal incidence to match the anatomical plane in which the vessels lie.

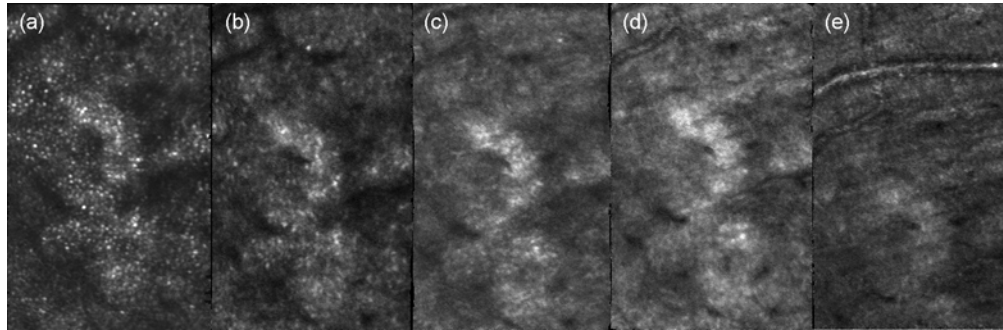


Fig. 8. tAOSLO images of lesions at various retinal depths from the cone mosaic (a) and progressively more superficial to the bottom of the nerve fiber layer (e). Each image consists of ~ 8 aligned and co-added frames. The frame dimensions are $\sim 0.8 \times 1$ deg.

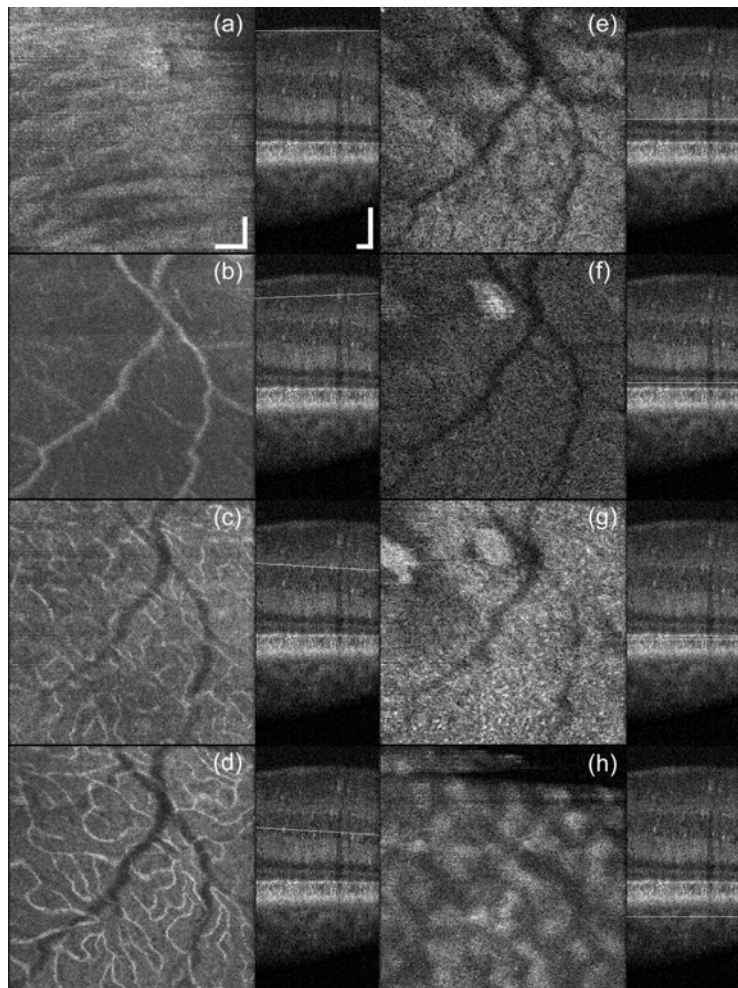


Fig. 9. AO-SDOCT montage of retinal layers. *En-face* images were constructed from OCT raster scan. Corresponding layer in cross-sectional scan are shown to the right of each *en face* image. (a) Nerve fiber layer (fibers bundles just visible running slightly off horizontal), (b) large retinal vessels in the ganglion cell layer, (c) small capillaries between inner plexiform and inner nuclear layers, (d) small capillaries at base of inner nuclear layer, (e) posterior outer plexiform layer (top of lesions), (f) photoreceptor outer segments, (g) photoreceptor inner segments, (h) choroid. Scale bar = $100 \mu\text{m}$.

The retinal layers from the nerve fibers (Fig. 9a) through the choroid (Fig. 9h) are shown. Because the focus was set to the photoreceptor layer and its thickness is relatively shallow, the contrast of the individual nerve fiber bundles in Fig. 9a is not large. However, note that the angular orientation of the fibers matches that shown in Fig. 8e. Figure 9b-d show retinal vessels in the anterior layers (Fig. 9b: ganglion cell layer; Fig. 9c: junction between inner plexiform and inner nuclear layers; Fig. 9d: posterior inner nuclear layer). The reflectance profile of the smallest capillary diameter in Fig. 9d measures $\sim 3 \mu\text{m}$ FWHM, although the actual vessel diameter is probably slightly larger than this. Fig. 9e shows that the disruption caused by the lesions extends into the outer plexiform layer. This fact is not evident in the cross-sectional image in Fig. 7. Fig. 9f shows the top of the lesions near the external limiting membrane. There does appear to be some structure in the lesions, although the integrity of a photoreceptor layer is not as clear in this view as it is in Fig. 8a. Fig. 9g shows the photoreceptor cone mosaic, albeit distorted by lateral eye movements. Note that both the AO-SDOCT scans of Fig. 9g and the AOSLO scans of Fig. 8a show disruption of the cone mosaic in the same circumferential regions around the lesions. Finally, Fig. 9h shows the large vessels in the choroid. Because of limited depth penetration, it is not clear that lesion disruption extends into the choroid, although the cross-sectional scan of Fig. 7 suggests that it does not.

It should be clear from Figs. 7-9 that both the AOSLO and AO-SDOCT provides information on lesion morphology and retinal structure that the other does not. Together, they allow several different views of a particular target. Future studies include configuration of the Indiana University AOSLO for acquisition of SDOCT scans on a clinical population with AMD and other retinal diseases [14].

5. CONCLUSION

We have presented the design, performance characterization, and initial human subject testing of a compact clinical adaptive optics spectral domain optical coherence tomography system. Simultaneous high-contrast wide-field confocal LSLO imaging allows retinal targets or structures to be selected and monitored. AO correction reduces the RMS wavefront error to $< 0.1 \mu\text{m}$ and increases the SDOCT image SNR to 3-10 dB for most subjects. Visualization of the smallest retinal capillaries in the inner nuclear layer is demonstrated. The performance of the system in comparison to an AOSLO is presented. The system is suitable for imaging a wide variety of retinal conditions. Future plans include integration of a SDOCT detection path into the AOSLO at Indiana University, studies of retinopathy of prematurity at Children's Hospital Boston, and an investigation of laser damage thresholds and mechanisms with AO-generated near diffraction-limited beams.

ACKNOWLEDGEMENTS

This work was supported by U.S. Air Force contracts FA8650-04-M-6514 and FA8650-05-C-6552.

REFERENCES

1. J. Liang, D. R. Williams, and D. T. Miller, "Supernormal vision and high-resolution retinal imaging through adaptive optics," *J. Opt. Soc. Am. A* 14, 2884-2892 (1997).
2. A. Roorda and D. R. Williams, "The arrangement of the three cone classes in the living human eye," *Nature* 397, 520-522 (1999).
3. A. Roorda, F. Romero-Borja, W. I. Donnelly, H. Queener, T. Hebert, and M. Campbell, "Adaptive optics scanning laser ophthalmoscopy," *Opt. Express*, 10, 405-412 (2002).
4. J. Martin and A. Roorda, "Direct and Noninvasive Assessment of Parafoveal Capillary Leukocyte Velocity," *Ophthalmol.*, 112, 2219-2224, (2005).
5. J. Martin and A. Roorda, "Direct and Non-invasive Parafoveal Microvascular Density and Foveal Avascular Zone Measurement," *ARVO Abstract* 3505, (2006).
6. D. C. Gray, W. Merigan, J. I. Wolfing, B. P. Gee, J. Porter, A. Dubra, T. H. Twietmeyer, K. Ahamd, R. Tumber, F. Reinholz, and D. R. Williams, "In vivo fluorescence imaging of primate retinal ganglion cells and retinal pigment epithelial cells," *Opt. Express*, 14, 7144-7158, 2006, <http://www.opticsinfobase.org/abstract.cfm?URI=oe-14-16-7144>.

7. F. Romero-Borja, K. Venkateswaran, A. Roorda, and T. Hebert, "Optical slicing of human retinal tissue in vivo with the adaptive optics scanning laser ophthalmoscope," *Appl. Opt.*, 44, 4032-4040, (2005).
8. B. Hermann, E. J. Fernandez, A. Unterhuber, H. Sattmann, A. F. Fercher, W. Drexler, P. M. Prieto, and P. Artal, "Adaptive-optics ultrahigh-resolution optical coherence tomography," *Opt. Lett.*, 29, 2142-2144 (2004).
9. R. J. Zawadzki, S. M. Jones, S. S. Olivier, M. Zhao, B. A. Bower, J. A. Izatt, S. Choi, S. Laut, and J. S. Werner, "Adaptive-optics optical coherence tomography for high-resolution and high-speed 3D retinal in vivo imaging," *Opt. Express*, 13, 8532-8546 (2005).
10. Y. Zhang, B. Cense, J. Rha, R. S. Jonnal, W. Gao, R. J. Zawadzki, J. S. Werner, S. Jones, S. Olivier, and D. T. Miller, "High-speed volumetric imaging of cone photoreceptors with adaptive optics spectral-domain optical coherence tomography," *Opt. Express*, 14, 4380-4394 (2006).
11. C. E. Bigelow, N. V. Iftimia, R. D. Ferguson, T. E. Ustun, B. Bloom, and D. X. Hammer, "Compact Multimodal Adaptive Optics Spectral Domain Optical Coherence Tomography Instrument for Retinal Imaging," *J. Opt. Soc. Am. A (Special Issue on Advances in Retinal Imaging)*, in press.
12. D. X. Hammer, R. D. Ferguson, T. E. Ustun, C. E. Bigelow, N. V. Iftimia, R. H. Webb, "Line-scanning laser ophthalmoscopy," *J. Biomed. Opt.*, 11, 041126 (2006).
13. D. X. Hammer, N. V. Iftimia, C. E. Bigelow, B. Bloom, R. D. Ferguson, and T. E. Milner, "Three-dimensional tracker for spectral domain optical coherence tomography," in Coherence Domain Optical Methods and Optical Coherence Tomography in Biomedicine XI, Eds., J. G. Fujimoto, J. A. Izatt, and V. V. Tuchin, paper 6429-38, 2007.
14. S. A. Burns, R. Tumber, A. E. Elsner, R. D. Ferguson, and D. X. Hammer, "Large Field of View, Modular, Stabilized, Adaptive-Optics-Based Scanning Laser Ophthalmoscope," *J. Opt. Soc. Am. A (Special Issue on Advances in Retinal Imaging)*, in press.